Monthly Notices
of the
ROYAL ASTRONOMICAL SOCIETY

MNRAS **480,** 2153–2164 (2018)
Advance Access publication 2018 July 24

doi:10.1093/mnras/sty1963

Investigating the rotational phase of stellar flares on M dwarfs using K2 short cadence data

L. Doyle,[1,2]★ G. Ramsay,[1] J. G. Doyle,[1] K. Wu[3] and E. Scullion[2]

[1]*Armagh Observatory and Planetarium, College Hill, Armagh BT61 9DG, UK*
[2]*Mathematics, Physics and Electrical Engineering, Northumbria University, Newcastle upon Tyne NE1 8ST, UK*
[3]*Mullard Space Science Laboratory, UCL, Holmbury St. Mary, Dorking, Surrey RH5 6NT, UK*

Accepted 2018 July 19. Received 2018 July 19; in original form 2017 November 21

ABSTRACT

We present an analysis of K2 short cadence data of 34 M dwarfs which have spectral types in the range M0–L1. Of these stars, 31 showed flares with a duration between ∼10 and 90min. Using distances obtained from *Gaia* DR2 parallaxes, we determined the energy of the flares to be in the range $\sim 1.2 \times 10^{29}$–6×10^{34} erg. In agreement with previous studies we find rapidly rotating stars tend to show more flares, with evidence for a decline in activity in stars with rotation periods longer than ∼10 d. The rotational modulation seen in M dwarf stars is widely considered to result from a starspot which rotates in and out of view. Flux minimum is therefore the rotation phase where we view the main starspot close to the stellar disc centre. Surprisingly, having determined the rotational phase of each flare in our study we find none show any preference for rotational phase. We outline three scenarios which could account for this unexpected finding. The relationship between rotation phase and flare rate will be explored further using data from wide surveys such as NGTS and TESS.

Key words: stars: activity – stars: flare – stars: low-mass – stars: magnetic field.

1 INTRODUCTION

M dwarfs make up 70 per cent of the stars in the solar neighbourhood. They are small, cool main-sequence stars with temperatures in the range of 2400–3800K and radius between 0.20–0.63 $R_\odot$ (Gershberg 2005). For stars with spectral type later than M4 it is thought their interiors are fully convective (Hawley et al. 2014). However, since these stars have no tachocline (a boundary zone between the radiative and convective zones) the star would not be expected to have a significant magnetic field if it was generated in the same manner as in the Sun. Some late M dwarfs *do* show strong flaring activity, highlighting a lack of understanding regarding the origins of their activity.

Over the years several models have been developed to account for the presence of a magnetic field in stars which are fully convective. Durney, De Young & Roxburgh (1993) propose a dynamo generated by a turbulent velocity field causing the generation of chaotic magnetic fields. Chabrier & Küker (2006) explore the possibility of an α^2 dynamo which can generate large-scale magnetic fields. However, this question still remains unresolved and the mechanism for producing a long lived magnetic field in late-type M dwarfs is still unknown.

One method of probing the magnetic field in these late-type stars is to investigate flares using them as a proxy for magnetic activity. In the case of well observed solar flares the correlation between magnetic field in active regions is very clear (Fletcher et al. 2011). Stellar flares are a phenomena which have been studied for a century. Some of the first detailed optical observations of stellar flares on M dwarfs were made by Bopp & Moffett (1973) and Gershberg & Shakhovskaya (1983). Amongst the first X-ray observations of stellar flares were made by Heise et al. (1975) using *EXOSAT* who detected an X-ray flare from the M4.5V star YZ CMi. Since then, the physics of stellar flares has been studied by many over the years and in the full energy range from γ-rays to radio frequencies.

More recently, the *Kepler* mission allowed almost uninterrupted observations of stars lasting many months, or in some cases years (Borucki et al. 2010). One particularly well studied flare star was GJ 1243 (KIC 9726699) which showed many flares especially when it was observed with a cadence of 1 min [short cadence (SC) mode; Ramsay et al. (2013); Hawley et al. (2014)]. This star has a spectral type of M4 making it an interesting example of a star which is on the cusp of having a fully convective core. Hawley et al. (2014) analysed the *Kepler* data of GJ 1243 to identify classical and complex flares, finding correlations between flare energy, amplitude, duration, and decay time. However, following the failure of two of *Kepler's* gyroscopes, it was re-purposed as K2 (Howell et al. 2014) observing targets along the ecliptic plane.

M dwarfs can show considerable amplitude variations in their light curves which have been explained by the presence of large dominant starspots on the surface moving in and out of view as

★ E-mail: Lauren.Doyle@Armagh.ac.uk

the star rotates. These amplitude variations in brightness represent one way of determining the stars rotation period and have produced accurate values of rotation periods for thousands of low-mass stars observed by *Kepler*/K2. Using K2 data Stelzer et al. (2016) observed 134 M dwarfs and focused on the relation between magnetic activity and stellar rotation. They found a difference between slow and fast rotating M dwarfs where after a period of approximately 10 d there is an abrupt change in activity. This would suggest a link between activity and rotation but, with the majority of targets being observed in long cadence (LC) (30 min) mode, short duration flares could not be detected leading to a bias against detecting short duration flares.

In solar physics the relationship between sunspots and solar flaring activity has been studied for decades and it is generally accepted that these two phenomena are closely related. Guo, Lin & Deng (2014) carried out a statistical study on the dependence of flares in relation to sunspots and rotational phase in the 22nd and 23rd solar cycles, respectively. They found the occurrence of X-class flares was in phase with the solar cycle hence, flares closely follow the same 11 yr cycle as sunspots. Maehara et al. (2017) investigated the correlation between starspots and superflares on solar-type stars using *Kepler* observations and identified starspots based on the rotational phase of the brightness minima in the light curve showing superflares tend to originate from a larger starspot area.

Despite the extensive work over the years, one area which has not been investigated in depth is the rotational phase distribution of flares in M dwarfs. If the analogy between the physics of solar and stellar flares holds and these events occur from active regions which typically host spots, then we would expect to see a correlation between starspots and flare occurrence. A small number of stars have been studied to determine whether there is a correlation between stellar rotation phase and number of flares, but so far nothing has been found. Ramsay et al. (2013), Hawley et al. (2014), Lurie et al. (2015), and Ramsay & Doyle (2015) examine the phase distribution of the flares in a small sample of M dwarf stars using *Kepler*/K2. Each of the stars show flares at all rotational phases despite there being clear rotational modulation present in their light curves. There was no evidence for a correlation between rotational phase and number of flares.

This poses the question; do flares show any preference for rotational phase in M dwarfs in general? It is expected that more flares would occur during the minimum of the rotational modulation when the spot is most visible. If this is not the case, then which mechanisms are responsible and what is causing the generation of flares in these active stars? In this paper, we look at a sample of M dwarf stars which have been observed in SC by K2. By analysing the flare and stellar properties of this group of stars we aim to address some of the questions surrounding the rotational phase distribution of the flares.

2 KEPLER/K2

2.1 Overview

Kepler was launched in 2009 and studied the same 115 square degree patch of sky just north of the Galactic plane for 4 yr, providing extensive photometric data for over 100 000 stars (Koch et al. 2004). The data obtained by Kepler have revolutionized the study of astrophysics especially in the field of exoplanets where it is responsible for finding the majority through the transit method. In addition, *Kepler* data have also revolutionized the fields of Asteroseismology, the number of stars with known rotation periods and interacting binaries. *Kepler* also provided the means to study stellar flares due to the high precision and length of the light curves. *Kepler* can operate in two observation modes, SC 1 min exposure and LC 30 min exposure.

We began a study of late-type flare stars towards the end of the *Kepler* mission. However, this ended with the loss of two of *Kepler*'s reaction wheels. New life was given to the mission when it was repurposed as K2 which began taking observations in 2014 June where fields are observed along the ecliptic for a duration of ∼70–80 d each (Howell et al. 2014). This study of late-type dwarfs using K2 SC data will allow us to study the flare properties of these stars in greater detail.

2.2 Data reparation

Because of the way K2 is pointed, the center of the stellar point spread function typically moves by ∼1 pixel over the course of 6 h (Van Cleve et al. 2016). Without applying a photometric correction the resulting error on a light curve can be considerably higher than for *Kepler*. For instance, for stars in the 10–11 mag range, *Kepler* gave an rms of 18 parts per million (ppm). For K2 the uncorrected rms is 170 ppm. Amongst the first to provide readily available corrected data were (Vanderburg & Johnson 2014), who were able to bring the rms for 10–11 mag stars down to 31 ppm.

A number of other groups have developed software which corrects for the instrumental effects which are present in raw K2 data. Not all of these techniques are suitable for SC mode data and some approaches can remove astrophysical effects. We have used the corrected K2 data using the EPIC Variability Extraction and Removal for Exoplanet Science Targets (`EVEREST`) pipeline (Luger et al. 2016) in all but one star in our sample. (For GJ 1224 observed in Field 9 we obtained the SC light curve from Andrew Vandenburg.)

Each photometric point has raw and corrected fluxes and a '`QUALITY`' flag. This is of particular importance when trying to find events such as flares which could, in principal, be mistaken for an instrumental effect. The `EVEREST` pipeline keeps the original flag definitions which were used in *Kepler*, but adds additional 'bit values'. For instance, bits '23' and '25' could be detector anomalies but could also be events such as eclipses or flares (Luger et al. 2016, 2017).

In searching for photometric variations longer than the typical duration of flares, such as the stellar rotation period, we were cautious and removed all events which did not conform to `QUALITY = 0`. When we searched for flares we removed photometric points, which were identified as bad in the *Kepler* Archive Manual[1] and points corresponding to bit values which were clearly identifying times when the spacecraft thruster was used such as bit value 20 and 21. We kept points which had bit values 23 and 25.

3 OUR K2 LATE DWARF SAMPLE

To create our sample of stars we took all the sources observed in SC with K2 in fields 1–9 (observations made between 2014 May and 2016 July) and cross referenced them with `SIMBAD`,[2] removing all stars which were not of spectral type M0 or later. In addition, those stars classed as BY Dra stars were removed from our sample since many of them are in binaries or triples and are therefore, not conducive to investigating stellar activity on single stars before and after the M4 spectral sub-type. The remaining stars

[1] https://archive.stsci.edu/kepler/manuals/archive_manual.pdf
[2] http://simbad.u-strasbg.fr/simbad

were then cross referenced with the EPIC catalogue and those which showed characteristics of a giant (e.g. have a radii $>1R_{\odot}$) were also removed. Stars which were too faint to show a clear detection in the K2 thumb print image were also removed from our sample.

This left us with a sample of late-dwarf stars observed with K2 in SC mode, consisting of 33 M dwarfs and one L dwarf. Of this sample of stars, 32 per cent were classed as known flare stars in the SIMBAD catalogue. They range in spectral type and mass from M0 to L1 and 0.58 to 0.08 $M_{\odot}$. Each target has been observed for ∼70–80 d producing a near continuous light curve over this period. The significance of SC data is it allows flares with a duration of a few minutes to be detected, giving a more comprehensive and robust overview of stellar activity. In addition, the wide range of spectral types provides a broader insight into how magnetic activity can vary in M dwarfs as a whole. The properties of the stars in our sample, including spectral type, previously known rotation period, mass, distance, and magnitude are shown in Table 1.

4 ROTATION PERIOD

From our sample of 34 stars, only five have rotation periods previously recorded in the literature, see Table 1. The two most important factors in determining the level of activity in a low-mass star are age and rotation period. The rotation period can be determined from low-mass stars if they have starspots whose rotation can produce a change in brightness as the starspots are expected to be darker than the photosphere (in the same way as sunspots). More recently, Karoff et al. (2018) compared the characteristics of the solar analogue star HD173701 with the Sun and found that metallicity could also be important factor in setting activity levels. How this results in a stronger dynamo is still unclear.

We first set out to determine or constrain the rotation period from the K2 data. The method used to determine the rotation period is initially through the Lomb–Scargle (LS) periodogram. We define $\phi = 0.0$ as the rotational phase where the flux is at a minimum and is first obtained by eye. For stars with a modulation period longer than 10 d we derive the rotation period, $P_{\rm rot}$, from the LS periodogram and fold the light curve to obtain a phase folded light curve. For stars where $P_{\rm rot} < 10$ d, we are able to refine $P_{\rm rot}$, and the time T_0, which defines the first minimum, by phasing and folding sections of the light curve taken from the start, middle, and end. This iterative procedure allows $P_{\rm rot}$ and T_0 to be determined more accurately than the LS periodogram alone. This gives us a mean folded light curve for our sample and is used during the analysis of flaring activity on the targets. The uncertainty on the rotation period is estimated by determining the full width at half max (FWHM) of the corresponding peak on the power spectrum.

We show the stellar rotation period derived for our sample using K2 data in Table 2: they range from 0.21 d to greater than 70 d. There are six stars in our sample where the amplitude modulation was incomplete and therefore it was only possible to say the rotation period is greater than the observation length, i.e. greater than 70 d. A further two stars had no apparent modulation in their light curve (possibly because they lack a large starspot). We find no correlation between rotation period and spectral type. For instance, stars with a rotation period less than 1 d have spectral types in the range M0–M8.5. Other examples of rapid rotation in late-type active stars include the M7 dwarf 2MASS J0335+23 (Gizis et al. 2017), which has a very rapid rotation period of 0.22 d, which is presumably due to its young age (24 Myr). Gizis et al. (2017) find 22 flares in the K2 light curve of 2MASS J0335+23 showing it is active.

Taking a sample of ∼12 000 main-sequence stars observed using *Kepler*, Nielsen et al. (2013) found M dwarfs had a median period of 15.4 d, although with a considerable spread in the overall distribution. Out of all of our stars only a handful show rotation periods which are not in agreement with the literature (compare column 7 in Table 1 with column 2 in Table 2). For some objects, the difference can be substantial, for e.g., HG 7−26 (EPIC 210317378) had a reported period of 0.192 d (Newton et al. 2016) compared to 24.5 d as derived from the K2 data, although the source is also classed as a 'non-detection or undetermined detection' in the catalogue of Newton et al. (2016). This underlines the need for a continuous sequence of photometric measurements, such as provided by K2, to reliably determine rotation periods.

5 FLARE IDENTIFICATION

The flare identification process was completed using Flares By EYE (FBEYE), a suite of IDL programs created by J.R.A. Davenport (Davenport et al. 2014). FBEYE allows users to manually classify flares present in the light curve via an interactive display. We are therefore able to determine for each flare the peak time, start time, end time, flux peak, and equivalent duration. The light curves which we used for this process were complete, meaning all photometric points were used regardless of their quality flag due to potential flaring events having quality flags which are not zero. The EVEREST quality flags and FBEYE flare list were then compared directly to assess the likelihood of the flare being a real event. Any photometric point with quality flags which were a result of thruster firing or known instrumental effects were removed from further analysis. Any point which had a flag of EVEREST bits 23 and 25 (which may have been due to cosmic rays or a real stellar flares) were kept. Events which consisted of only one photometric point were removed and events which did not have profiles consistent with being a likely stellar flare (i.e. sharp rise and exponential decay) were also removed.

The data for each star were analysed in a consistent manner and for each star we show the number of flares, the range in the duration and amplitude of the flares in Table 2. In addition, we have added the normalized flare number which represents the number of flares expected on each star if the observation duration was 78.3 d. The duration of each flare was calculated from the start and stop times and the amplitude represents the flux peak of each flare all which were obtained from the output of FBEYE. Sources 2MASS J0831+1025, 2MASS J0909+1940, and L 762−51 did not show any flares and were omitted from Table 2 – these sources did also not show complete rotational cycles and so the rotational periods could not be determined.

We show some examples of flares from GJ 3225 (EPIC 210758829) in Fig. 1. Of particular interest is the largest flare from this star with a normalized flux peak of 4.32 (equivalent of 1.6 mag), where a rapid rise (approximately 1 min) and clear slow decay (approximately 10 min) can be seen which, is similar to a classical stellar flare profile.

It is expected to find greater flare activity on stars with shorter rotation periods. This is the case with this particular sample of M dwarfs (Fig. 2); however, the star with the most flares does not have the fastest rotation. After a rotation period of approximately 10 d there is a drop off in the number of flares seen on the star, which is consistent with the findings of Stelzer et al. (2016). In order to create a complete picture of this sample of M dwarfs the ages of the stars would need to be determined, as although the activity of the stars depends on rotation, this in turn depends on age.

Table 1. The properties of the M stars which are included in our survey where all data comes from the K2 EPIC catalogue (Huber et al. 2016), with the exception of the following. References for spectra: [1] Hawley, Gizis & Reid (1996); [2] Reid et al. (2008); [3] Reid et al. (2004); [4] Lépine & Gaidos (2011); [5] Kraus & Hillenbrand (2007), [6] Schmidt et al. (2010), [7] Gray et al. (2003); [8] Davison et al. (2015); [9] Lépine et al. (2013); [10] Kirkpatrick, Henry & McCarthy Jr (1991); [11] Faherty et al. (2009); [12] Pesch (1968); [13] Alonso-Floriano et al. (2015); [14] Stephenson (1986); [15] Cruz & Reid (2002); [16] Shkolnik, Liu & Reid (2009).

Name	EPIC ID	K2 field	RA (J2000)	Dec. (J2000)	SpT	P d	M $M_\odot$	R $R_\odot$	$T_{\rm eff}$ (K)	log g (cgs)
LHS 2420	201611969	1	11:31:32.845	+02:13:42.86	M2.5V [9]		0.319	0.301	3740	4.977
LP 804−27	205204563	2	16:12:41.781	−18:52:31.83	M3V [7]		0.445	0.391	3930	4.86
GJ 3954	205467732	2	16:26:48.160	−17:23:33.6	M4.5V		0.304	0.286	3772	4.995
IL Aqr	206019387	3	22:53:16.7	−14:15:49.3	M4V [1]	95	0.21	0.22	3472	5.07
LP 760−3	206050032	3	22:28:54.401	−13:25:17.86	M6.5V [10]		0.09	0.113	2617	5.271
2MASSI J2214−1319	206053352	3	22:14:50.707	−13:19:59.080	M7.5 [11]		0.078	0.098	2211	5.349
Wolf 1561 A	206262336	3	22:17:18.9	−08:48:12.5	M4V + M5V [1]		0.22	0.23	3495	5.06
HG 7−26	210317378	4	3:52:34.340	+11:15:38.807	M1 [12]	0.192	0.396	0.358	3788	4.917
NLTT 12593	210434433	4	4:07:54.80	+14:13:00.7	M2.5V [13]	1.073	0.424	0.382	3844	4.896
G 6−33	210460280	4	3:45:54.83	+14:42:52.1	M1.5 [9]		0.511	0.454	4028	4.821
LP 415−363	210489654	4	4:20:47.988	+15:14:09.073	M4V [13]	82.6	0.391	0.351	3751	4.917
MCC 428	210579749	4	3:43:45.247	+16:40:02.166	M0V [14]		0.504	0.449	3898	4.836
GJ 3225	210758829	4	03:26:45.0	+19:14:40.1	M4.5V [1]	0.454	0.13	0.15	3027	5.19
2MASS J0326+1919	210764183	4	03:26:44.5	+19:19:31.0	M8.5V [2]		0.08	0.10	2192	5.34
LP 414−108	210811310	4	04:10:38.1	+20:02:23.5	M0.5V+M0.5V [3]		0.43	0.37	3971	4.89
LP 357−206	210894955	4	3:55:36.90	+21:18:48.30	M5 [15]	7.916	0.240	0.248	3550	5.014
2MASSJ0335+2342	211046195	4	3:35:02.087	+23:42:35.61	M8.5V [16]	0.472	0.084	0.106	2432	5.310
LT Tau	211069418	4	03:42:56.5	+24:04:58.1	M3.5V [4]		0.32	0.30	3675	4.97
V497 Tau	211077349	4	03:42:02.9	+24:12:36.3	M3V [4]		0.44	0.40	3876	4.87
V692 Tau	211082433	4	03:56:30.4	+24:17:18.8	M4-5V [4]		0.26	0.26	3567	5.03
V631 Tau	211112686	4	03:44:24.8	+24:46:06.3	M1V [4]	3.27	0.37	0.34	3700	4.93
V* MY Tau	211117230	4	3:44:27.293	+24:50:38.26	M0 [16]	0.4	0.427	0.381	3811	4.894
2MASS J0831+1025	211329075	5	08:31:56.0	+10:25:41.7	M9V [2]		0.08	0.10	2209	5.34
GJ 3508	211642294	5	8:37:07.961	+15:07:45.5257	M3V [9]		0.427	0.385	3861	4.892
LP 426−35	211945363	5	08:57:15.4	+19:24:17.7	M5V [5]		0.35	0.32	3738	4.96
2MASS J0909+1940	211963497	5	09:09:48.2	+19:40:42.9	L1 [6]		0.08	0.10	2098	5.36
AX Cnc	211970427	5	08:39:09.9	+19:46:58.9	M2 [5]	4.854	0.45	0.41	3881	4.87
2MASS J0831+2024	212009427	5	08:31:29.9	+20:24:37.5	M0V [5]	1.55	0.58	0.51	4116	4.78
2MASS J0839+2044	212029094	5	08:39:18.1	+20:44:21.3	M1V [5]		0.34	0.32	3785	4.96
L 762−51	212285603	6	13:45:50.7	−17:58:05.6	M3.5V [1]		0.31	0.30	3646	4.99
LP 737−14	212518629	6	13:16:45.47	−12:20:20.4	M3.5V [13]		0.281	0.273	3577	5.005
BD-05 3740	212776174	6	13:38:58.7	−06:14:12.5	M0.5V [7]		0.45	0.40	3847	4.88
2MASSI J1332−0441	212826600	6	13:32:24.427	−4:41:12.690	M7.5 [6]		0.079	0.101	2264	5.328
GJ 1224	228162462	9	18:07:32.927	−15:57:46.46	M4V [8]		0.14			

6 FLARE ENERGIES

To determine the energy of the stellar flares, the quiescent luminosity of the star, L_*, must be calculated in the *Kepler* bandpass. To construct a template spectral energy distribution for each star we used PanStarrs magnitudes g, r, i, and z (see Table A1). The PanStarrs magnitudes (Chambers et al. 2016) represent the mean quiescent magnitude of the star calculated over an average of multiple measurements. This ensures the effects of flares or rotation has been removed from the magnitudes. We fitted a polynomial to the Panstarrs data and determined the flux in the *Kepler* bandpass in the same manner as Kowalski et al. (2013). The quiescent luminosity is then computed by multiplying the flux by $4\pi d^2$, where the distance (d) to the stars has been determined by inverting the parallax from the *Gaia* Data 2 release (Gaia Collaboration et al. 2016, 2018; see Table 3). We also used the Bayesian analysis approach as described by Astraatmadja & Bailer-Jones (2016) and implemented in the STILTS suite of software (Taylor 2006), and find that, as expected for sources within 200 pc, the distances and errors determined using the inversion and the Bayesian approach are entirely consistent.

The energy of the flares, $E_{\rm flare}$, can then be determined by the multiplication of the luminosity of the star, L_*, in erg s^{-1} and the equivalent duration, t, in seconds. The equivalent duration (Gershberg 1972) is defined as the area under the flare light curve in units of seconds, which is different to the flare duration, and is obtained through the FBEYE suite of programs. FBEYE uses a Trapezoidal summation of the area under the flare light curve which is converted into seconds.

A wide range of flare energies are seen in the 31 flaring M dwarfs. The most energetic flare is observed in V497 Tau at $\sim$5.9 $\times$ 10^{34} erg and the flare with the lowest energy at $\sim$1.3 $\times$ 10^{29} erg is seen in IL Aqr. The range of energies seen in the sample are comparable to energies seen in other work similar to this. Using *Kepler* data, Hawley et al. (2014) showed flares with energies in the range of $\sim$2 $\times$ 10^{28}−2 $\times$ 10^{33} erg on the M dwarf GJ 1243. Other stars in their sample were consistent with this but less extreme. In addition, Lurie et al. (2015) investigated the M5 binary system GJ 1245 also using 9 months of SC *Kepler* data, finding a total of 1288 flares on both stars with an energy range of $\sim$1 $\times$ 10^{30}−1 $\times$ 10^{33} erg.

Table 2. For the stars in our survey which show flaring activity we indicate their observed rotation period; the number of flares together with their duration, amplitude, and energy. Since the length of each observation differs by a small amount, we have included a normalized flare number which is the number of flares expected on each star if the observation duration was 78.3 d.

EPIC ID	Rotation period (P_{rot}) d	No. of flares	Normalized flare no.	Duration range min	Amplitude range Flux	$log(E_{Kp})$ ergs
201611969	>70	15	14.33	11.8–35.3	0.0009–0.0095	31.17–32.18
205204563	42:	5	4.72	8.83–20.6	0.0003–0.0030	29.12–31.05
205467732	1.321 ± 0.021	221	205.35	8.83–91.2	0.0003–1.3694	30.60–33.49
206019387	>70	47	39.27	10.8–81.4	0.0004–0.0151	30.01–31.77
206050032	>70	17	14.21	10.8–32.4	0.0274–0.6937	31.25–32.52
206053352	–	8	6.78	11.8–30.4	0.2254–6.7031	31.19–32.27
206262336	9.6 ± 1.2	237	194.73	8.78–46.1	0.0018–1.2462	29.45–33.06
210317378	24.5:	7	6.06	12.8–21.6	0.0069–0.0582	31.39–32.28
210434433	47:	4	3.49	14.7–24.5	0.0041–0.0207	31.02–32.11
210460280	45:	1	0.87	29.42	0.0024	31.47
210489654	>80	24	20.90	10.8–39.2	0.0037–0.0632	31.06–32.28
210579749	23:	4	3.43	12.8–42.2	0.0014–0.0027	31.37–31.95
210758829	0.4539 ± 0.0027	197	170.68	8.78–106	0.0023–4.3192	30.09–33.46
210764183	0.966 ± 0.011	10	8.77	8.78–45.9	0.2365–5.1922	31.95
210811310	33:	2	1.75	10.8	0.0013–0.0028	30.88–31.16
210894955	0.726 ± 0.006	18	15.81	10.8–30.4	0.0455–2.3884	30.65–32.58
211046195	0.2185 ± 0.0006	16	14.02	0.98–2888	0.0437–4.5665	31.15–34.57
211069418	0.8177 ± 0.0086	104	90.48	8.78–63.8	0.0101–0.4138	31.65–33.81
211077349	0.6992 ± 0.0061	64	55.75	8.78–75.6	0.0142–3.8455	31.69–34.77
211082433	0.3447 ± 0.0015	123	107.23	8.78–71.6	0.0097–0.4683	31.17–33.51
211112686	0.7639 ± 0.0073	53	46.34	8.78–94.0	0.0103–0.4311	31.99–34.24
211117230	0.398 ± 0.002	38	32.72	8.83–76.5	0.0045–0.2136	32.08–34.28
211642294	52:	5	4.49	20.6–103	0.0023–0.0196	31.15–34.42
211945363	>70	8	7.39	10.8–31.2	0.0025–0.0231	31.19–31.98
211970427	4.38 ± 0.24	51	47.31	8.78–64.8	0.0101–0.3572	32.04–34.09
212009427	1.556 ± 0.029	75	69.34	8.78–76.5	0.0068–0.0967	32.14–34.29
212029094	20.22 ± 5.03	3	2.78	14.7–22.5	0.0019–0.0087	31.19–31.66
212518629	80:	1	0.96	27.46	0.0106	31.46
212776174	18.35 ± 5.03	7	6.58	10.8–20.6	0.0007–0.0038	31.21–31.99
212826600	–	7	6.79	12.8–41.2	0.0015–0.8707	32.15–33.31
228162462	3.9 ± 0.2	424	355.31	8.78–165	0.0015–0.8707	29.32–32.74

Notes. For a handful of sources the apparent modulation period is longer than the observation length meaning only an lower limit to the rotation period could be determined. For stars with no evidence for a modulation no rotation period could be determined.

For comparison, these large-scale flares of order of 10^{34} erg are equivalent to extremely large X-class flares, in terms of the solar flare GOES classification. In Table 4, we note the median energy of the flares for each star.

7 ROTATIONAL PHASE

Stars with starspots can show a periodic change in brightness as the stars rotates due to the starspots being cooler than the surrounding photosphere. If stellar flares originate from the starspot, one might naively expect more flares would be seen at rotation minimum where the starspot is most visible. However, if a star has a low rotation angle (i.e. one of its rotation poles is close to being face on), spots near the pole would be visible at all phases, and flares would be seen at all rotation phases. To investigate this further, we now set out to determine the rotation phase of the flares we identified in the previous section.

For this analysis, stars with rotation periods shorter than the observation length were selected. Due to this, eight of the sources are omitted from this analysis and any further investigations due to the K2 light curve showing incomplete modulation which lead to the rotation period being unable to be confirmed. We phase folded and binned the light curves using the rotation period shown in Table 2 and the phase zero calculated previously, yielding rotation cycles covering all of the K2 light curve showing a minimum at $\phi = 0.0$. We show the resulting phase folded and binned light curves in Fig. B1. Flares are present at practically all rotational phases for all stars. In many cases there are high-energy flares present at rotation maximum, where we would expect the starspot to be least visible. Many of the light curves show a roughly sinusoidal modulation suggesting the presence of one prominent starspot, although several sources, such as Wolf 1561 A (which is in a triple system) show evidence for a second starspot. The fact that all the stars shown in Fig. B1 show a clear modulation suggests we are not observing them at low rotation angles.

In order to determine whether the phase distribution of the flares is random we used the χ^2 statistic. Flares were split up into high and low energy with a cut-off determined by the median energy of all flares from each star. In addition, the rotational phase was split into 10 bins and χ^2 was determined for each star in the low, high, and all energy categories, where the degrees of freedom, ν, is 9. Table 4 shows the results for both high- and low-energy flares and also all flares in each star overall. Regarding low, high, and all flare categories, none of the stars show a preference for rotational phase even at a 2σ confidence level. Therefore, there is no evidence for the flares having any preference for rotational phase, which surprisingly indicates many flares may not originate from the large starspot. We now go on to investigate possible causes for this.

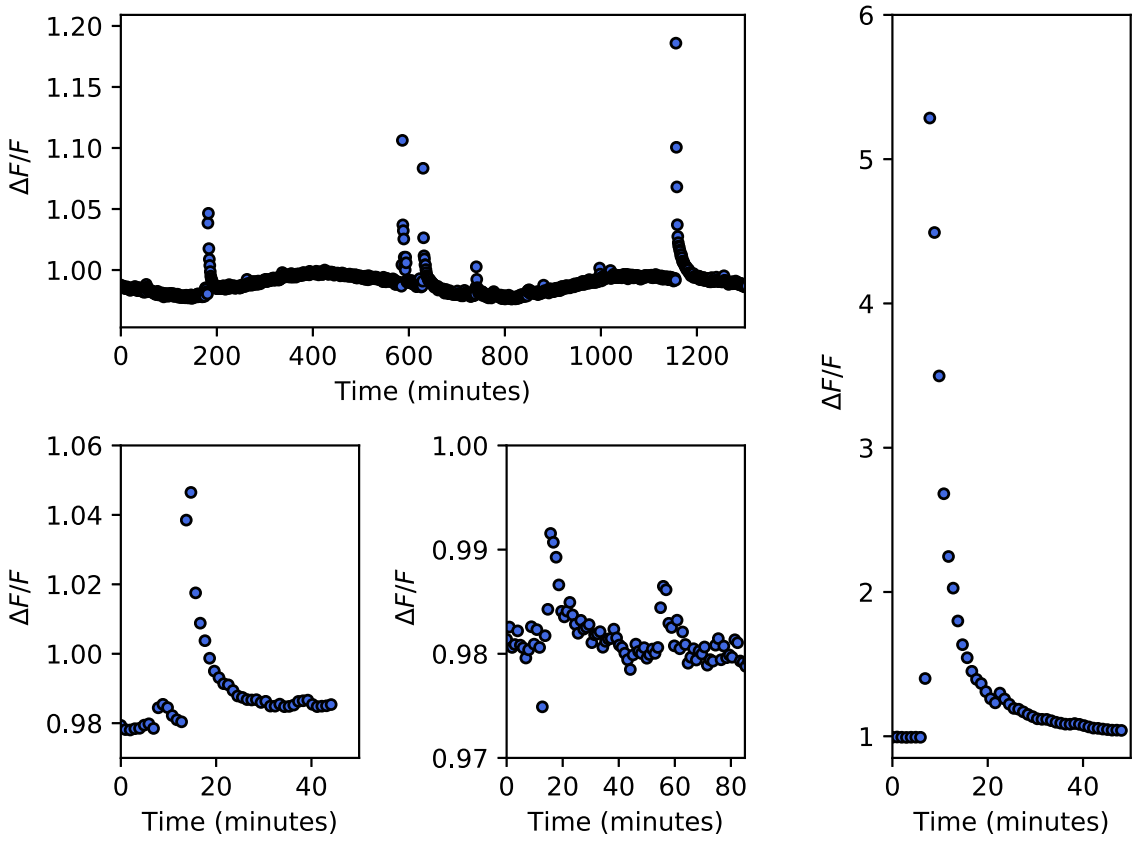

Figure 1. A sample of flares of varying magnitude from the flare star GJ 3225 (EPIC 210758829) a M4.5 star with a rotation period of 0.45 d. The top plot shows a small section of the light curve of the star demonstrating the frequency of the flares and also the range in magnitude. Far right is the largest flare seen in the K2 light curve of this star with a peak normalized flux of 4.32. The bottom two plots show smaller amplitude, short duration flares which dominate the light curve.

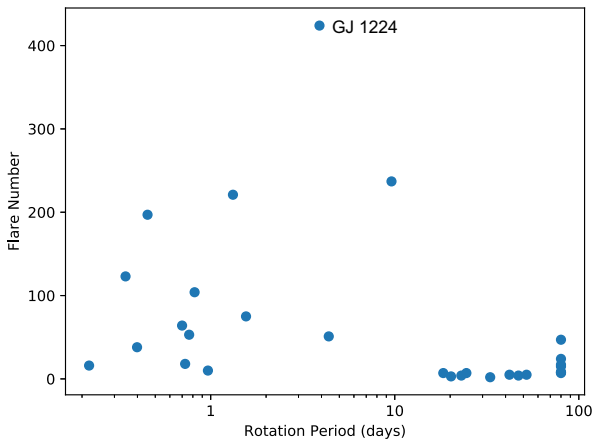

Figure 2. The number of flares as a function of the rotation period for all stars showing flaring activity. As other studies have found, stars with rotation periods longer than ∼10 d are less active. The most active star is GJ 1224, $P_{\rm rot}$= 3.9 d. There are six sources to the very right-hand side which represent the stars with rotation periods >70 d.

8 DISCUSSION

We have analysed flaring activity from a sample of 31 M dwarfs covering a range of spectral types using K2 SC data. We derived (or placed lower limits on) the rotation periods of 29 of these stars using the K2 light curves, many for the first time. In addition to this we used the flare characteristics (energy, duration, and phase of the rotation cycle) to compute a statistical analysis of flares of this sample.

It is known, from previous studies (e.g. Mohanty & Basri 2003; McLean, Berger & Reiners 2012), that faster rotating stars show greater flaring activity. Moreover, activity drops for stars with rotation periods >10 d (Stelzer et al. 2016). Our findings are consistent with these results. However, our work has identified an area which has not previously been studied in great detail. If flares originate from the same starspot which causes the rotational modulation, we would expect to observe a clear correlation of flares with rotational phases: this is not what we observe. None of the stars in our sample show evidence for flares being preferentially seen at certain rotation phases. This result is unexpected and seems to point to the conclusion that the majority of flares do not originate from the prominent starspot.

Where do flares originate on these active stars and how are they generated? We consider three possible scenarios. Firstly, there is the potential of magnetic interaction with a second star in a binary system. It is possible for interactions between the M dwarf and a binary companion causing increased magnetic activity between the stars and in turn the generation of flares at locations other than a dominant starspot. As summarized by Kouwenhoven et al. (2009), 30–40 per cent of M dwarfs are members of a binary system. For late M dwarfs and brown dwarfs this drops to 10–30per cent. This suggests less than a dozen of our sample will be in a binary system

Table 3. Parallaxes along with their associated errors from *Gaia* Data release 2 (Gaia Collaboration et al. 2016, 2018) which are then inverted to calculate the distances to the stars in our sample. The errors on the quiescent luminosity include the error on the distance and the PanStarrs magnitude. Three of our stars did not have parallaxes in the *Gaia* DR2 catalogue and so these distances were taken from the EPIC Catalogue (Huber et al. 2016) and marked with an asterisk.

Name	Parallax mas	Parallax error mas	Distance pc	$log(L_{star})$ erg s^{-1}
201611969	35.48	0.06	28.18 ± 0.04	31.679 ± 0.006
205204563	68.78	0.12	14.54 ± 0.03	31.266 ± 0.007
205467732	–	–	28.3*	30.88
206019387	213.87	0.08	4.676 ± 0.002	30.864 ± 0.001
206050032	91.89	0.09	10.88 ± 0.01	30.564 ± 0.004
206053352	25.3	0.2	39.47 ± 0.31	29.261 ± 0.032
206262336	89.20	0.13	11.21 ± 0.02	30.385 ± 0.006
210317378	28.59	0.06	34.97 ± 0.08	31.119 ± 0.009
210434433	32.36	0.06	30.90 ± 0.06	31.188 ± 0.008
210460280	27.61	0.04	36.22 ± 0.06	31.389 ± 0.006
210489654	34.72	0.15	28.80 ± 0.12	31.011 ± 0.016
210579749	58.01	0.05	17.24 ± 0.01	31.661 ± 0.003
210758829	55.20	0.09	18.12 ± 0.03	30.330 ± 0.007
210764183	34.12	0.42	29.31 ± 0.36	28.936 ± 0.049
210811310	19.07	0.04	52.45 ± 0.12	31.477 ± 0.009
210894955	34.69	0.13	28.83 ± 0.11	29.763 ± 0.015
211046195	19.53	0.15	51.21 ± 0.40	29.988 ± 0.032
211069418	8.13	0.65	122.9 ± 9.9	31.355 ± 0.321
211077349	7.34	0.07	136.3 ± 1.3	31.306 ± 0.038
211082433	12.62	0.17	79.24 ± 1.09	31.131 ± 0.055
211112686	7.47	0.05	133.9 ± 0.9	31.623 ± 0.028
211117230	7.58	0.05	131.9 ± 0.9	32.016 ± 0.027
211642294	56.10	0.06	17.82 ± 0.02	31.307 ± 0.004
211945363	–	–	37.7*	31.41
211970427	5.28	0.15	189.3 ± 5.4	31.721 ± 0.113
212009427	5.43	0.04	184.2 ± 1.2	32.083 ± 0.026
212029094	5.39	0.06	185.3 ± 2.1	31.513 ± 0.045
212518629	45.5	1.2	21.98 ± 0.58	30.832 ± 0.105
212776174	41.31	0.05	24.21 ± 0.03	32.022 ± 0.005
212826600	–	–	109*	30.49
228162462	125.59	0.07	7.962 ± 0.004	30.156 ± 0.002

and hence binarity is unlikely to play a prominent role in resolving this question.

Our second scenario is that magnetic interaction could occur with a planet orbiting the M dwarf. Dressing & Charbonneau (2015) present an updated occurrence rate for planets orbiting early M dwarfs as 2.5 planets per M dwarf star. Depending on the number of planets orbiting the host star (and the mass, radius, and magnetic field of the planet), it could be induced magnetic activity between the star-planet system which causes the increased flaring activity. However, both the first and second scenario would depend on a small separation between the orbiting star or planet to allow for any magnetic interaction.

We now consider the likely separation between the photosphere of the M dwarf and the magnetic interaction region. In the multiscale field scenario of Yadav et al. (2015), only the large-scale field (lower order multiple) would interact with any orbiting planets and the location of any 'null points' (where the global topology of the magnetic field changes) would be in a transitional region where the long range dipole field becomes weaker than the quadrupole (higher order) field. As the null point induced by the planet is also associated with the dipole field it cannot be too close to the stellar surface. Moreover, this kind of null point would not be associated with the dominant stellar spot (which is not created by the dipole field component). Furthermore, the reconnection region would not easily be eclipsed by the star so, it is natural that we do not see any correlation with the phases and the flares.

A third possibility is the presence of polar spots on the M dwarf. Depending on the viewing geometry and the relative inclination of the rotational and magnetic moment axes of the star, polar spots could be seen at all phases, interacting with emerging active regions and spot free regions as the star rotates, causing continuously visible flaring activity. The Sun does not possess polar spots, so the presence of polar spots on M dwarfs would support the view that the generation of the magnetic field in these stars differs from that of the Sun.

Despite the absence of polar spots on the Sun, Schrijver & Title (2001) model the formation of polar spots on rapidly rotating (6 d) Sun-like stars due to the poleward migration of the magnetic field. Their models predicted very active stars possessing polar caps with topologies of one polarity encircling another. This magnetic configuration could generate very large filaments, flares, and coronal mass ejections. Despite the differences between rapidly rotating Sun-like stars and fully convective low-mass stars, the work of Schrijver & Title (2001) highlighted that a global poloidal field and a shear underneath/next to it in a perpendicular direction, a local dynamo can occur. Hence, this could lead to flare activity.

We now go on to consider the formation of polar spots on fully convective low-mass stars. Yadav et al. (2015) investigated the conditions necessary for formation of polar spots in convection driven

Table 4. For the stars shown in Fig. B1 (with the exception of EPIC 210460280 which has only one flare) we show the χ^2_ν value for whether each rotation phase bin (split into 10) had flares which were randomly distributed by phase. We split the flares into low and high energy where the cut-off is determined by the median energy of all the flares for each star. None of the stars in our sample show a preference for flares at a certain rotational phase.

EPIC	Median energy (erg)	Reduced Chi-squared		
		Low	High	All
205204563	9.5×10^{30}	0.78	2.00	1.00
205467732	2.3×10^{31}	1.17	1.17	0.55
206262336	6.5×10^{30}	0.92	1.13	0.61
210317378	6.2×10^{31}	0.78	1.22	0.97
210434433	4.9×10^{31}	0.89	0.89	1.22
210579749	3.9×10^{31}	0.89	0.89	0.67
210758829	6.7×10^{30}	1.14	0.30	0.62
210764183	2.3×10^{31}	1.44	1.00	1.11
210811310	1.1×10^{31}	1.00	1.00	2.00
210894955	1.9×10^{31}	1.10	1.35	0.47
211046195	3.7×10^{32}	0.33	0.78	0.78
211069418	1.8×10^{32}	0.93	1.33	0.65
211077349	3.1×10^{32}	0.82	0.82	1.15
211082433	1.2×10^{32}	1.11	0.39	0.72
211112686	4.8×10^{32}	0.58	1.21	1.18
211117230	1.9×10^{33}	0.87	0.99	0.69
211642294	8.6×10^{31}	0.78	0.89	1.00
211970427	5.5×10^{32}	0.82	0.82	1.24
212009427	7.8×10^{32}	0.54	0.81	0.33
212029094	2.5×10^{31}	1.00	0.89	1.52
212776174	4.3×10^{31}	1.22	0.78	0.97
228162462	4.6×10^{30}	0.83	0.48	0.94

dynamos. This directly applies to many stars in our sample as they are fully convective, and a magnetic field driven by the α^2 dynamo mechanism. As a result of their parameter study, they determine three key features for large spot formation in fully convective stars: (i) rotation driven convection, (ii) many scale heights in the convection zone, (iii) a dynamo producing an axial-dipole field. All of our stars posses these properties and so, this could be the solution to the key problem noticed in the rotational phase of the flares?

Yadav et al. (2015) also show a self-consistent distributed dynamo can spontaneously generate high-latitude dark spots when a large-scale magnetic field, generated in the bulk of the convection zone, interacts with and locally quenches flow near the surface. This is similar to findings reported by Schrijver & Title (2001), who explored the migration of surface magnetic fields towards the poles. Rapid rotation is vital for the formation of such dark polar spots. However, if there is a global polaroidal field and a shear underneath/next to it in a perpendicular direction, a local dynamo can occur.

Such flare activity from the polar regions could be caused by large-scale 2D vortices within the poloidal fields which thread through the temperature inversion layer (in the polar regions) acting in a similar way to charged particles when they experience a force across the field lines perpendicular to their motion. When such 2D vortices are formed they may wind up the field line with them and when these eddies encounter the rim of the polar cap, (whose axis is not aligned with the rotation axis of the star), magnetic reconnection may occur generating flares.

We have outlined three scenarios to explain the lack of rotational phase preference for flares in our M dwarf sample. In order to test our theories further we would need to compare results from stars with low and high inclination. Davenport, Hebb & Hawley (2015) and Silverberg et al. (2016) reported observations of GJ 1243 which has a high rotation inclination and a high latitude spot. With many thousands of flares being detected, no correlation with its 0.59 d rotational period was found. A sample of stars with well-defined inclination values is the next step in allowing us to distinguish between the three scenarios to explain our main result.

9 CONCLUSIONS

Previous observations of activity levels in fast and slow rotators suggest a rotation-dependent transition in the magnetic properties of the atmosphere of M dwarfs, where the transition corresponds to approximately 10 d. Using K2 SC observations of a sample of 34 M dwarfs, we have found an interesting result. There is no correlation between the rotation phase and the number of flares. Given these stars all show significant rotational modulation amplitude due to a starspot, this is a surprise.

New wide field surveys which are red sensitive will be suited to exploring these issues in greater detail and with larger sample sizes. For instance, the New Generation Transit Survey (NGTS) (Wheatley et al. 2017) has a field of view of 96 square degree and is red sensitive. Although its prime goal is the detection of Neptune and super-Earth size exo-planets it will obtain long duration light curves of many red dwarfs. The *Transiting Exoplanet Survey Satellite* (*TESS*) (Ricker et al. 2015) was launched on the 18th April 2018. *TESS* will be sensitive to stars brighter than $V\sim12$ and will have 27 d observation blocks covering $24^\circ \times 96^\circ$ of sky with a cadence of 1 min for many objects. It will therefore be suitable to address our key questions. Furthermore, *TESS* will provide photometric precision which is one order of magnitude greater than Kepler/K2, therefore, allowing a better evaluation of the low energy part of the flare frequency/flare energy distribution.

ACKNOWLEDGEMENTS

We thank Andrew Vanderberg for kindly detrended these K2 short cadence data and the K2 Guest Observer Office Team for their support and enthusiasm for the mission. Armagh Observatory and Planetarium are core funded by the Northern Ireland Government through the Dept. for Communities. LD acknowledges funding from an STFC studentship. This work presents results from the European Space Agency (ESA) space mission *Gaia*. *Gaia* data is being processed by the *Gaia* Data Processing and Analysis Consortium (DPAC). Funding for the DPAC is provided by national institutions, in particular the institutions participating in the *Gaia* MultiLateral Agreement (MLA). The Gaia mission website is https://www.cosmos.esa.int/gaia. The Gaia archive website is https://archives.esac.esa.int/gaia.

The Pan-STARRS1 Surveys (PS1) and the PS1 public science archive have been made possible through contributions by the Institute for Astronomy, the University of Hawaii, the Pan-STARRS Project Office, the Max–Planck Society, and its participating institutes, the Max Planck Institute for Astronomy, Heidelberg, and the Max Planck Institute for Extraterrestrial Physics, Garching, The Johns Hopkins University, Durham University, the University of Edinburgh, the Queen's University Belfast, the Harvard-Smithsonian Center for Astrophysics, the Las Cumbres Observatory Global Telescope Network Incorporated, the National Central University of Taiwan, the Space Telescope Science Institute, the National Aeronautics and Space Administration under Grant No. NNX08AR22G issued through the Planetary Science Division of the NASA Science

Mission Directorate, the National Science Foundation Grant No. AST-1238877, the University of Maryland, Eotvos Lorand University (ELTE), the Los Alamos National Laboratory, and the Gordon and Betty Moore Foundation.

REFERENCES

Alonso-Floriano F. et al., 2015, A&A, 577, A128
Astraatmadja T. L., Bailer-Jones C. A. L., 2016, ApJ, 833, 119
Bopp B. W., Moffett T., 1973, ApJ, 185, 239
Borucki W. J. et al., 2010, Science, 327, 977
Chabrier G., Küker M., 2006, A&A, 446, 1027
Chambers K. C. et al., 2016, preprint (arXiv:1612.05560)
Cruz K. L., Reid I. N., 2002, AJ, 123, 2828
Davenport J. R. et al., 2014, ApJ, 797, 122
Davenport J. R. A., Hebb L., Hawley S. L., 2015, ApJ, 806, 212
Davison C. L. et al., 2015, AJ, 149, 106
Dressing C. D., Charbonneau D., 2015, ApJ, 807, 45
Durney B. R., De Young D. S., Roxburgh I. W., 1993, Sol. Phy., 145, 207
Faherty J. K., Burgasser A. J., Cruz K. L., Shara M. M., Walter F. M., Gelino C. R., 2009, 15th Cambridge Workshop on Cool Stars, Stellar Systems and the Sun, Vol. 1094, Am. Inst. Phys., New York, p. 517
Fletcher L. et al., 2011, SSRv, 159, 19
Gaia Collaboration Brown A. G. A., Vallenari A., Prusti T., de Bruijne J. H. J., Babusiaux C., Bailer-Jones C. A. L., 2018, preprint (arXiv:1804.09365)
Gaia Collaboration et al., 2016, A&A, 595, A1
Gershberg R. E., 1972, Ap&SS, 19, 75
Gershberg R. E., 2005, Solar-type activity in main-sequence Stars. Springer Science & Business Media, Berlin
Gershberg R. E., Shakhovskaya N. I., 1983, Ap&SS, 95, 235
Gizis J. E., Paudel R. R., Mullan D., Schmidt S. J., Burgasser A. J., Williams P. K. G., 2017, ApJ, 845, 1
Gray R. O., Corbally C. J., Garrison R. F., McFadden M. T., Robinson P. E., 2003, AJ, 126, 2048
Guo J., Lin J., Deng Y., 2014, MNRAS, 441, 2208
Hawley S. L., Gizis J. E., Reid I. N., 1996, AJ, 112, 2799
Hawley S. L., Davenport J. R., Kowalski A. F., Wisniewski J. P., Hebb L., Deitrick R., Hilton E. J., 2014, ApJ, 797, 121
Heise J., Brinkman A., Schrijver J., Mewe R., Gronenschild E., Den Boggende A., Grindlay J., 1975, ApJ, 202, L73
Howell S. B. et al., 2014, PASP, 126, 398
Huber D. et al., 2016, ApJS, 224, 2
Karoff C. et al., 2018, ApJ, 852, 46
Kirkpatrick J. D., Henry T. J., McCarthy D. W., Jr, 1991, ApJS, 77, 417
Koch D. G. et al., 2004, Optical, Infrared and Millimeter Space Telescopes, 5487, 1491
Kouwenhoven M., Brown A., Goodwin S., Zwart S. P., Kaper L., 2009, A&A, 493, 979
Kowalski A. F., Hawley S. L., Wisniewski J. P., Osten R. A., Hilton E. J., Holtzman J. A., Schmidt S. J., Davenport J. R., 2013, ApJS, 207, 15
Kraus A. L., Hillenbrand L. A., 2007, AJ, 134, 2340
Lépine S., Gaidos E., 2011, AJ, 142, 138
Lépine S., Hilton E. J., Mann A. W., Wilde M., Rojas-Ayala B., Cruz K. L., Gaidos E., 2013, AJ, 145, 102
Luger R., Agol E., Kruse E., Barnes R., Becker A., Foreman-Mackey D., Deming D., 2016, AJ, 152, 100
Luger R., Kruse E., Foreman-Mackey D., Agol E., Saunders N., 2017, preprint
Lurie J. C., Davenport J. R., Hawley S. L., Wilkinson T. D., Wisniewski J. P., Kowalski A. F., Hebb L., 2015, ApJ, 800, 95
Maehara H., Notsu Y., Notsu S., Namekata K., Honda S., Ishii T. T., Nogami D., Shibata K., 2017, PASJ, 69
McLean M., Berger E., Reiners A., 2012, ApJ, 746, 23
Mohanty S., Basri G., 2003, ApJ, 583, 451
Newton E. R., Irwin J., Charbonneau D., Berta-Thompson Z. K., Dittmann J. A., West A. A., 2016, ApJ, 821, 93
Nielsen M. B., Gizon L., Schunker H., Karoff C., 2013, A&A, 557, L10
Pesch P., 1968, ApJ, 151, 605
Ramsay G., Doyle J. G., 2015, MNRAS, 449, 3015
Ramsay G., Doyle J. G., Hakala P., Garcia-Alvarez D., Brooks A., Barclay T., Still M., 2013, MNRAS, 434, 2451
Reid I. N. et al., 2004, AJ, 128, 463
Reid I. N., Cruz K. L., Kirkpatrick J. D., Allen P. R., Mungall F., Liebert J., Lowrance P., Sweet A., 2008, AJ, 136, 1290
Ricker G. R. et al., 2015, J. Astron. Telesc. Instrum. Syst., 1, 014003
Schmidt S. J., West A. A., Hawley S. L., Pineda J. S., 2010, AJ, 139, 1808
Schrijver C. J., Title A. M., 2001, ApJ, 551, 1099
Shkolnik E., Liu M. C., Reid I. N., 2009, ApJ, 699, 649
Silverberg S. M., Kowalski A. F., Davenport J. R. A., Wisniewski J. P., Hawley S. L., Hilton E. J., 2016, ApJ, 829, 129
Stelzer B., Damasso M., Scholz A., Matt S. P., 2016, MNRAS, 463, 1844
Stephenson C. B., 1986, AJ, 92, 139
Taylor M. B., 2006, in Gabriel C., Arviset C., Ponz D., Enrique S., eds, ASP Conf. Ser. Vol. 351, Astronomical Data Analysis Software and Systems XV, Astron. Soc. Pac., San Francisco, p. 666
Van Cleve J. E. et al., 2016, PASP, 128, 75002
Vanderburg A., Johnson J. A., 2014, PASP, 126, 948
Wheatley P. J. et al., 2017, MNRAS, 475, 4476
Yadav R. K., Gastine T., Christensen U. R., Reiners A., 2015, A&A, 573, A68

APPENDIX A: PANSTARRS MAGNITUDES

Table A1. For all the stars in our sample we present the corresponding PanStarrs magnitudes (Chambers et al. 2016) in the *g*, *r*, *i*, and *z* bands with errors which are also taken from the PanStarrs catalogue. These magnitudes are used to create a template spectrum of each star and used in the calculation of the quiescent *Kepler* luminosity.

Name	EPIC ID	*g*	*r*	*i*	*z*
LHS 2420	201611969	13.0682 ± 0.0010	11.7446 ± 0.0010	10.0773	10.6904 ± 0.1852
LP 804−27	205204563	12.2986 ± 0.0010	11.0668 ± 0.1391	9.8560 ± 0.1723	9.0415 ± 0.0378
GJ 3954	205467732	15.0310 ± 0.0034	13.7505 ± 0.0029	12.2592 ± 0.3998	11.1509 ± 0.0210
IL Aqr	206019387	11.0744 ± 0.0150	8.9746 ± 0.0692	8.4762 ± 0.0394	8.1422 ± 0.2303
LP 760−3	206050032	12.2150	11.5380	11.2720	11.1370
2MASSI J2214−1319	206053352	20.8604 ± 0.0406	19.4495 ± 0.0081	16.9408 ± 0.0041	15.7102 ± 0.0042
Wolf 1561 A	206262336	14.2094 ± 0.0001	13.5603 ± 0.0784	11.3962 ± 0.0352	10.4803 ± 0.0635
HG 7−26	210317378	14.3808 ± 0.0065	13.2037 ± 0.0107	12.1530 ± 0.0701	11.4553 ± 0.0371
NLTT 12593	210434433	13.6522 ± 0.0005	12.3198 ± 0.0010	11.9320	10.7620 ± 0.0397
G 6−33	210460280	12.5168 ± 0.0055	11.6516 ± 0.0404	12.2169 ± 0.0385	11.8217 ± 0.0991
LP 415−363	210489654	14.4373 ± 0.0057	13.3156 ± 0.0037	11.8085 ± 0.0385	13.3588 ± 0.0012
MCC 428	210579749	11.2964 ± 0.0520	10.0182 ± 0.0124	9.3745 ± 0.2068	8.5127 ± 0.0229
GJ 3225	210758829	15.5532 ± 0.0024	14.2847 ± 0.0037	12.5702 ± 0.0183	11.9246 ± 0.1065
2MASS J0326+1919	210764183	21.4785 ± 0.1072	19.7707 ± 0.0250	17.1323 ± 0.0032	15.7071 ± 0.0027
LP 414−108	210811310	13.7311 ± 0.0100	12.5716 ± 0.0599	12.3544 ± 0.1876	12.2010 ± 0.3246
LP 357−206	210894955	18.4372 ± 0.0077	17.1264 ± 0.0034	14.9935 ± 0.0013	14.0026 ± 0.0041
2MASS J0335+2342	211046195	19.5600 ± 0.0100	18.2366 ± 0.0054	15.6818 ± 0.0029	14.4760 ± 0.0047
LT Tau	211069418	16.8460 ± 0.0065	15.6460 ± 0.0035	14.2525 ± 0.0012	13.3161 ± 0.0017
V497 Tau	211077349	17.0385 ± 0.0053	15.7580 ± 0.0126	14.5928 ± 0.0049	14.0379 ± 0.0036
V692 Tau	211082433	16.7380 ± 0.0118	15.5423 ± 0.0052	13.8039 ± 0.0004	12.8970
V631 Tau	211112686	15.9072 ± 0.0060	14.7119 ± 0.0089	13.8246 ± 0.0100	13.3578 ± 0.0050
V* MY Tau	211117230	14.6712 ± 0.0068	13.5257 ± 0.0010	12.8800	12.4340
GJ 3508	211642294	12.3840 ± 0.0010	11.7487 ± 0.0461	10.0195 ± 0.0502	11.4547 ± 0.0000
LP 426−35	211945363	14.0742 ± 0.0024	13.3732 ± 0.4861	11.3541 ± 0.0010	11.9661 ± 0.0010
AX Cnc	211970427	16.6625 ± 0.0041	15.4590 ± 0.0008	14.2677 ± 0.0010	13.7382 ± 0.0034
2MASS J0831+2024	212009427	15.3423 ± 0.0041	14.1807 ± 0.0014	13.3870	13.0250 ± 0.0079
2MASS J0839+2044	212029094	17.0009 ± 0.0051	15.7975 ± 0.0017	14.7718 ± 0.0023	14.3082 ± 0.0030
LP 737−14	212518629	14.3029 ± 0.0051	13.0944 ± 0.0010	11.7148 ± 0.0400	12.1497 ± 0.0010
BD-05 3740	212776174	11.4172 ± 0.0406	9.2114 ± 0.0875	9.3707 ± 0.0523	9.1667 ± 0.0487
2MASSI J1332−0441	212826600	20.2436 ± 0.0221	18.7220 ± 0.0132	16.0798 ± 0.0023	14.7831 ± 0.0025
GJ 1224	228162462	14.1926 ± 0.0010	13.0493 ± 0.0098	11.1694 ± 0.0134	10.8942

APPENDIX B: LIGHT CURVES

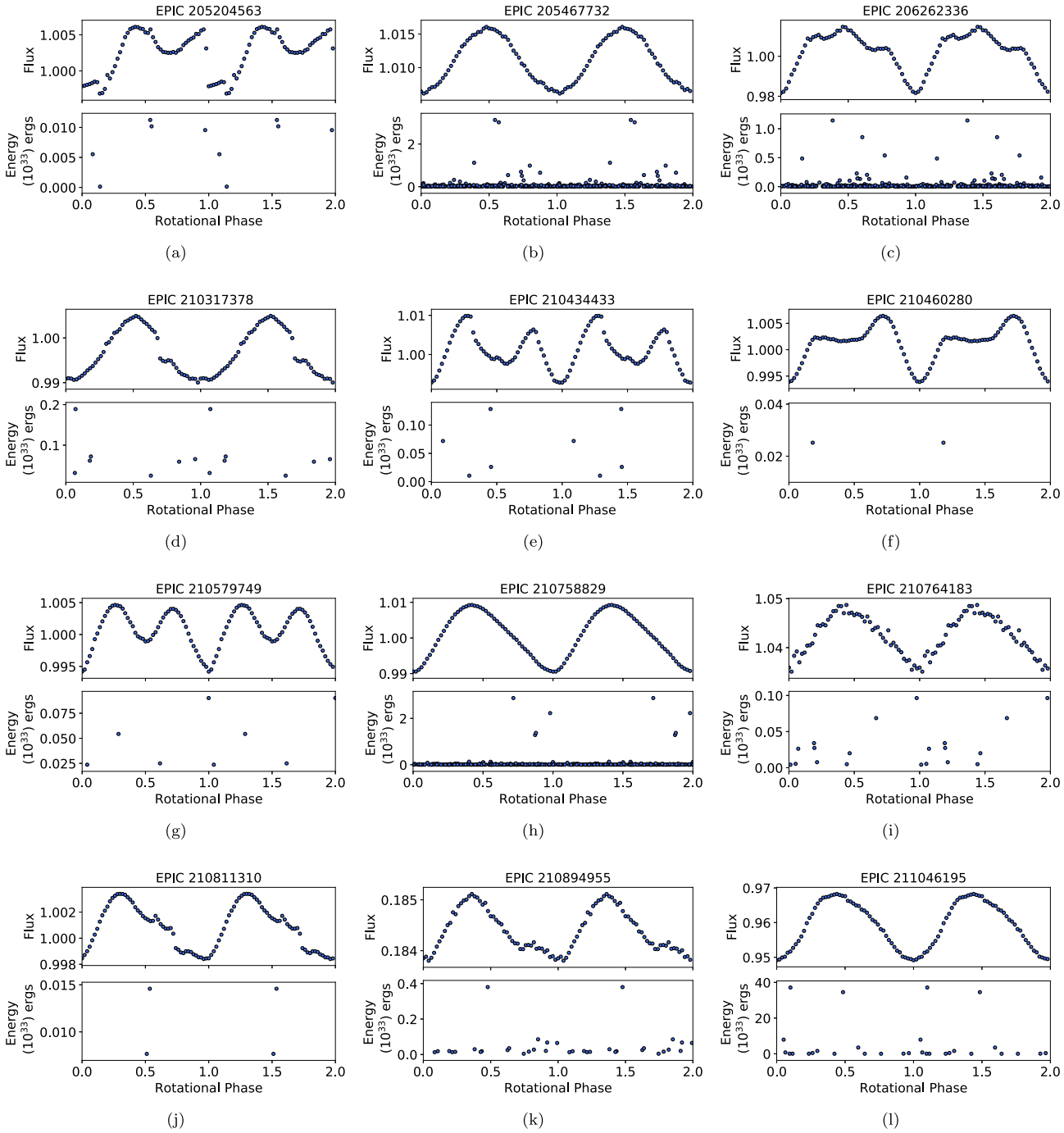

Figure B1. In the top panels we show the light curves of each star phased and binned on the rotation period such that there are 50 bins per rotation phase. In the bottom panels we show the phase of the flares with the energy. For each star we plot the data twice so they cover rotation phase 0.0–2.0, where 1.0–2.0 is simply a repeat of 0.0–1.0. The star shown in panel (a) shows three rotation cycles with a long term trend and the variation may indicate significant cycle to cycle variability.

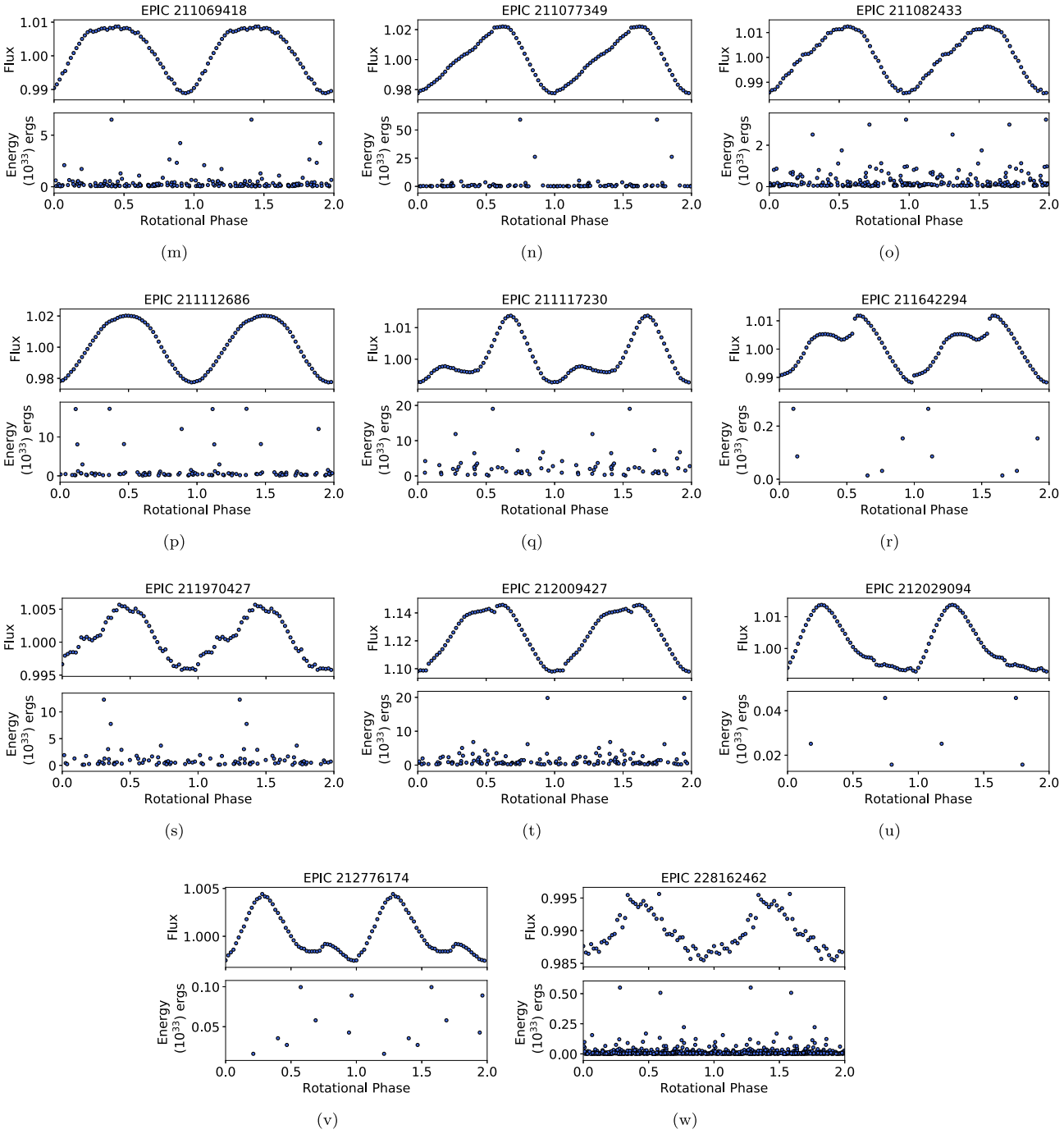

Figure B1. continued

This paper has been typeset from a TEX/LATEX file prepared by the author.